

Investigating the Effect of Tether Drag on System Efficiency  
of a KiteGen Stem Airborne Wind Energy Generator

Alexandre Veillerette

26<sup>th</sup> October 2023



Interim Report  
Mechanical Engineering MEng Individual Project 5  
MECE11006

## **Abstract**

This master's degree individual project investigates the impact of tether drag on kite power system efficiency. Existing analytical models often rely on oversimplified assumptions when assessing energy yield and system efficiency. Assumptions made regarding tether drag lead to errors that become more pronounced with increasing tether length, ultimately failing to align with real-world observations. This project will be conducted in collaboration with KiteGen, which emphasises the need to explain the disparities observed between their kite power systems and the existing analytical models. KiteGen will contribute valuable guidance to comprehending the real-world behaviour of kite power systems and will provide experimental data essential for model validation. The following interim report serves as a means to evaluate current progress, provide an overview of significant research in the field, define project goals, and outline the strategy to achieve these objectives. After an introduction on airborne wind energy and kite power systems, this interim report encompasses a literature review of current analytical models, followed by a project outline and timeline identifying key objectives of this project.

# Contents

<b>Abstract</b>	<b>ii</b>
<b>1 Introduction</b>	<b>1</b>
1.1 Tropospheric Wind . . . . .	1
1.2 Airborne Wind Energy . . . . .	2
1.3 KiteGen Stem Technology . . . . .	4
<b>2 Literature Review</b>	<b>5</b>
2.1 Upper Bound for Instantaneous Power . . . . .	5
2.2 Refined Crosswind Motion Laws . . . . .	6
2.3 Tether Flexibility . . . . .	7
2.4 Review of Assumptions . . . . .	9
<b>3 Project Plan</b>	<b>11</b>
3.1 Project Outline . . . . .	11
3.2 Project Timeline . . . . .	12
<b>References</b>	<b>17</b>

# 1 Introduction

## 1.1 Tropospheric Wind

Caused by the sun's uneven heating of the earth's surface, pressure differences in the atmosphere drive the movement of air. The use of wind energy dates back thousands of years, with evidence of sailing boats dating back 7,000 years [1], and the earliest windmills, panemones, emerging over 2,000 years ago [2]. In recent years, wind energy production has been growing at an annual rate of 9%, reaching a global capacity of 906 GW as of 2023 [3].

Wind energy is harnessed by converting the kinetic energy of the wind into mechanical and, subsequently, electrical power. The kinetic energy  $E_k$  of a fluid of mass  $m$  and velocity  $v$  can be expressed as:

$$E_k = \frac{1}{2}mv^2 \quad (1.1)$$

Taking air at speed  $V_w$  with mass flow rate  $\dot{m}$ , the kinetic power in the wind  $P_w$  can be shown to be:

$$P_w = \frac{1}{2}\dot{m}V_w^2 = \frac{1}{2}\rho_a A V_w^3 \quad (1.2)$$

Where  $\rho_a$  is the density of air and  $A$  is the area considered. Per unit area, this is expressed as wind power density  $\delta_w$ :

$$\delta_w = \frac{1}{2}\rho_a V_w^3 \quad (1.3)$$

From the surface to around 2000 meters, Earth's friction slows the wind, creating what is referred to as the boundary layer. Within this boundary layer, wind velocity increases with altitude, with velocity  $V_w$  at height  $z$  often modelled with the wind shear power law, in terms of reference velocity  $V_{ref}$  at height  $z_{ref}$  [4]:

$$V_w(z) = V_{ref} \left( \frac{z}{z_{ref}} \right)^\alpha \quad (1.4)$$

Where the shear index  $\alpha$ , typically between 0.1 - 0.4, is based on landscape properties, and affects the wind velocity profile within the boundary layer as well as the boundary layer height.

Whilst wind velocity  $V_w$  increases within the boundary layer, air density  $\rho_a$  decreases exponentially with altitude, following the barometric equation [5]:

$$\rho_a(z) = \rho_0 e^{-z/k} \quad (1.5)$$

With  $\rho_0$  being air density at ground level and  $k \approx 8330\text{ m}$ .

As seen in equation (1.3), wind power density varies linearly with density but cubically with wind speed, generally leading to increased power density with height. Although wind speed maxima can occur at the top of the boundary layer, wind speed generally increases with height above the boundary layer as well [6]. Consequently, wind power density increases with altitude within the troposphere, as shown in Figure 1.

Compared to 50-150 m, well within the boundary layer, where most conventional wind farms operate, wind power density was found to be 4 times higher at 500-1000 m, and 40 times higher at 10,000 m [6].

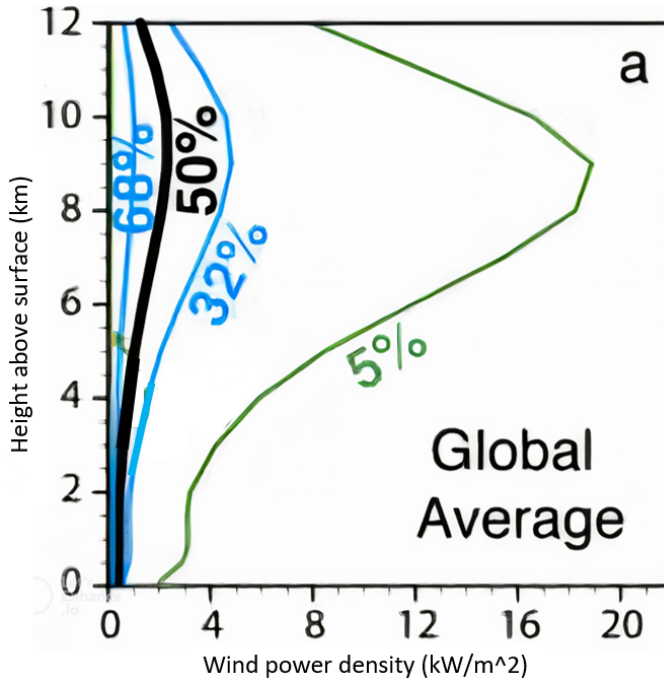


Figure 1: Wind power density exceeded for 5%, 32%, 50% and 68% of the time at varying height, global average. Adapted from [6].

With total atmospheric wind power estimated to be of 3,600 TW [7], the evident untapped potential of high altitude wind presents an opportunity which an increasing amount of organisations are attempting to exploit [4].

## 1.2 Airborne Wind Energy

While the idea of harvesting high altitude wind energy is not novel, research and development in this sector has only exploded in the past 20 years or so, primarily driven by improvements in material science and control technology [4]. Employing airborne wind energy (AWE) devices instead of conventional wind turbines yields several main advantages:

- Access to stronger and more consistent wind speeds.
- Structurally unconstrained sweep area.
- Lightweight and portable infrastructure.
- Capability for rapid and safe return to the ground.

The radically different system design implies cheaper and safer maintenance, as well as increased weather resilience. Unconstrained sweep area and access to a range of altitudes leads to an increased capacity factor [8], higher power density [9], and the lightweight infrastructure has an estimated embodied energy of 1% of conventional wind turbines [10], leading to a significantly higher ERoEI<sup>1</sup> [11]. AWE has the potential to disrupt the energy market, with conservative estimates for LCOE<sup>2</sup> falling within 20 – 50 £/MWh<sup>3</sup> by 2030 [9][12][13][4].

---

<sup>1</sup>Energy returned on energy invested.

<sup>2</sup>Levvelised cost of electricity.

<sup>3</sup>Converted to value of £ in 2023.

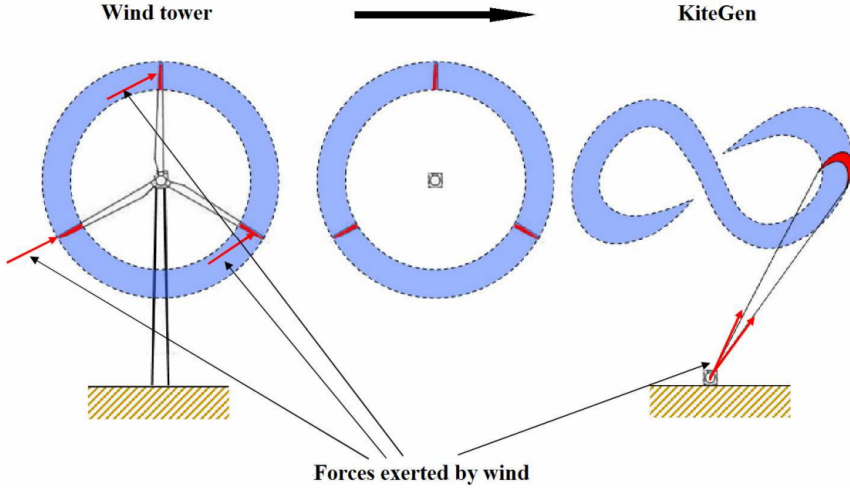


Figure 2: Illustration of basic concept of a KiteGen pumping kite generator [14].

A wide range of designs have been proposed to exploit tropospheric wind, including tethered kites, buoyant wind turbines, magnus effect generators, and tethered drones [15]. Compared to stationary systems, flying crosswind increases the aerodynamic forces acting on the airfoil, providing one or two orders of magnitude higher power [16]. Within crosswind devices, AWE devices can be broadly categorised as Fly-Gen and Ground-Gen, referring to the generation of electricity. In Ground-Gen devices, electrical energy is produced by transmitting mechanical power from the airborne device to the ground station through one or more tethers, where it is converted to electricity by a generator.

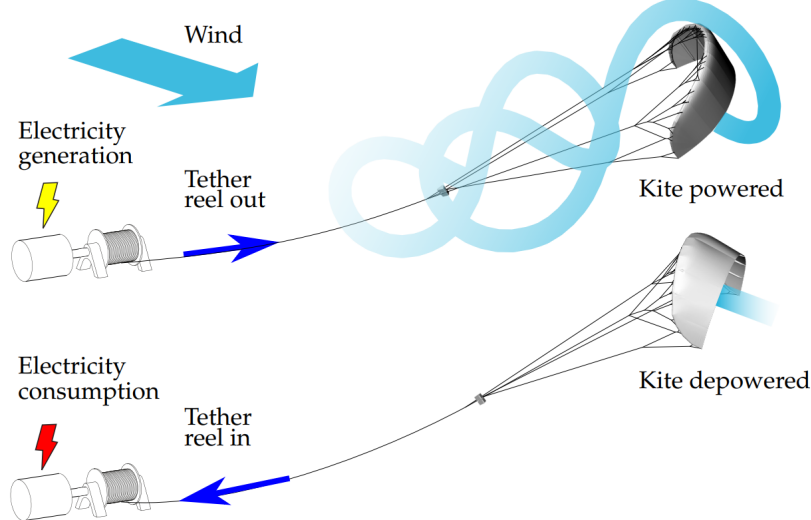


Figure 3: Illustration of pumping kite cycle [17].

Ground-Gen devices are lift-based devices driven by airfoils, either rigid or flexible, and energy is produced by either having a stationary or moving ground station. Since 80% of the energy produced by conventional wind turbines comes from the outer 20% of the blades [14], the core concept of Ground-Gen AWEs are to have a light airfoil, equivalent to the outer portion of a wind turbine's blade, fly crosswind at high speeds (Figure 2). Many flight and tether configurations have been

proposed, with current research in this area appearing to converge towards a pumping kite generator design<sup>4</sup>.

Pumping kite generators are AWE devices involving a power phase and a reel-in phase, shown in Figure 3. During the power phase, a kite is allowed to fly out in either circular or figure-of-eight motions across the wind (preferred as to avoid twisting of the tether [18]), at much higher velocities than the wind itself. The kite's lift produces a large pulling force, which is transmitted to the generator at the ground station. This is followed by using the generator as a motor to reel in the tether while controlling the kite to reduce the pulling force.

### 1.3 KiteGen Stem Technology

KiteGen propose two main AWE systems: the KiteGen Carousel, a Ground-Gen concept with multiple kites attached to a rotating station, and KiteGen Stem, which features a single crosswind pumping kite generator connected to a stationary ground station (Figure 4). The LCOE goals for these technologies are < 10 £/MWh and < 25 £/MWh, respectively<sup>5</sup> [19].



Figure 4: Illustration of KiteGen Stem AWE Device [20].

The KiteGen Stem technology was announced to have reached TRL8<sup>6</sup> in 2016 [20], and is the subject of this project. The design is highly scalable, with each device having a power capacity of 3 MW with a 13 m diameter base, for a total weight of 6 tonnes per MW. The system has the following main components:

- Airfoil: semi-rigid kite, taking advantage of the efficiency and durability of rigid airfoils while using the patented side-slip maneuver<sup>7</sup> during reel-in.
- Tether: two tethers connected to the kite, made from high tension polyethylene fibers.
- Control unit: between the kite and the ground station, controlling kite motion by varying tether length.
- Mechanical power converter: drum winch, gearbox, and motor/generator; mechanical power is kept constant by varying reel-out speed through the control unit.
- Electrical power converter: inverter, transformer, batteries, and other electrical components, placed in the ground station.
- Launching and landing systems: including stem structure to launch and land the kite

---

<sup>4</sup>A comprehensive review of AWE systems can be found at [15].

<sup>5</sup>Converted to value of £ in 2023.

<sup>6</sup>Technology readiness level

<sup>7</sup>Animation and demonstration of slip maneuver can be found at [21].

## 2 Literature Review

### 2.1 Upper Bound for Instantaneous Power

Following the first experiments dedicated towards the exploitation of high-altitude wind power in 1979 [4], Miles Loyd developed the first analytical model of crosswind kite power in 1980, laying the foundation for quantitative analysis of AWE [16].

By modelling a weightless kite flying at velocity  $\bar{V}_C$  perpendicular to wind  $\bar{V}_w$ , an analysis of the forces and velocities is done. Noting that the mechanical power  $P$  generated by pulling a tether with force  $T$  at reel-out velocity  $\bar{V}_L$  is equal to:

$$P = TV_L \quad (2.1)$$

The forces and velocities on the kite, as shown in Figure 5, are analysed to find a theoretical upper bound for mechanical power.

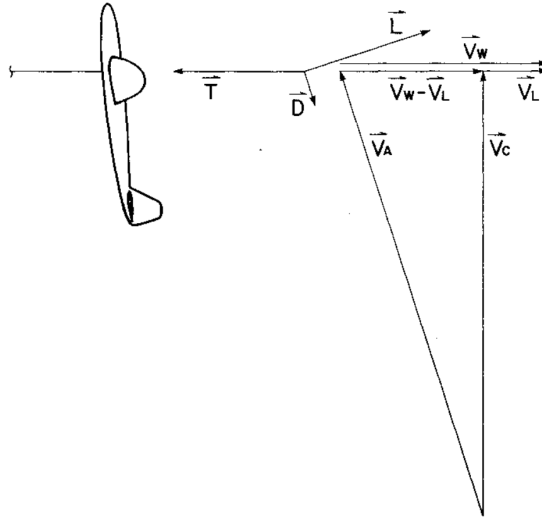


Figure 5: Diagram of forces and velocities acting on a kite in 2 dimensions [16].

Noting that the velocities and the forces form similar right angles, crosswind velocity  $\bar{V}_C$ :

$$V_C = (V_w - V_L)(L/D_k) \quad (2.2)$$

Where  $L$  is kite lift and  $D_k$  is kite drag. By then assuming that  $L \gg D_k$ , the angle formed is small, and  $\bar{V}_C \approx \bar{V}_A$ . Therefore:

$$V_A = (V_w - V_L)(L/D_k) \quad (2.3)$$

Following the same assumption,  $L \approx T$ , and mechanical power is expressed as:

$$P = LV_L \quad (2.4)$$

Since the aerodynamic lift of the kite is given by:

$$L = \frac{1}{2}\rho C_L A V_A^2 \quad (2.5)$$

Equations (2.3, 2.4, 2.5) are combined to find the maximum theoretical instantaneous mechanical power produced by a kite flying crosswind:

$$P = \frac{2}{27} \rho A V_w^3 C_L \left( \frac{L}{D_k} \right)^2 \quad (2.6)$$

Which occurs at the tether reel-out velocity  $V_L = \frac{1}{3}V_w$ . Noting that  $L/D_k = C_L/C_D$ , the maximum theoretical power can be expressed in terms of wind power density  $\delta_w$  (1.3), kite reference area  $A$ , lift coefficient  $C_L$ , and function  $F$ :

$$P = \delta_w A V_w^2 C_L F \quad (2.7)$$

Where:

$$F = \frac{4}{27} \left( \frac{C_L}{C_D} \right)^2 \quad (2.8)$$

Importantly, this theoretical upper bound for instantaneous energy production was obtained by modelling a kite perfectly perpendicular to the wind velocity  $\bar{V}_w$  in 2 dimensions, and the effect of tether drag was neglected. Equation (2.6), referred to as Loyd's formula, shows that the mechanical power  $P$ :

$$P \propto C_L \left( \frac{C_L}{C_D} \right)^2 \quad (2.9)$$

The aerodynamic efficiency  $C_L/C_D$  of the kite, also called the glide ratio, is therefore an important term for power maximisation.

## 2.2 Refined Crosswind Motion Laws

This initial analysis evolved through iterative consideration of additional factors. In an optimisation study on crosswind kite energy, the effect of the tether drag is considered, where it is assumed to add directly to the kite drag [22]. A new term, the effective glide ratio  $G_e$ , is introduced:

$$G_e = \frac{L}{D_k + F_f} \quad (2.10)$$

Where  $F_f$  is the tether drag. In a continued analysis, Lagrange's theorem is used to derive the equations of motion of the system in spherical coordinates [5]. The tether is modelled as a straight line, and assuming uniform wind velocity, the tether drag is found to be:

$$F_f = \frac{C_{D,t} \rho_a r d_t}{8} V_a^2 \quad (2.11)$$

Where  $C_{D,t}$  is the tether drag coefficient (assumed constant),  $r$  is the tether length, and  $d_t$  is the tether diameter.

An initial estimation of mechanical energy output for pumping kite generators by Argatov applies the case of equilibrium motion to the kite system in spherical coordinates [23]. The kite flies within a quarter sphere referred to as the flight envelope, and two new vectors are introduced:  $\bar{V}_C$ , the projection of apparent wind  $V_a$  on the plane orthogonal to the tether (equivalent to  $\bar{V}_C$  in Figure 2.6); and  $\bar{V}_{||}$ , the wind speed component orthogonal to the flight envelope (equivalent to  $\bar{V}_w$  in Figure 2.6).

The total forces acting on the kite are given as the sum of gravitational and aerodynamic forces, where the tether drag is once more assumed to directly contribute to the kite's aerodynamic forces. Continuing the analysis, the following equation is obtained:

$$|\bar{V}_C| = \bar{V}_{||} \frac{L}{D + F_f + F_w^{gra}} \quad (2.12)$$

Where  $F_w^{gra}$  is the component of the gravitational force in the direction of  $\bar{V}_C$ . This equation, referred to as the refined crosswind motion law, states that the crosswind speed of a kite is greater than the wind speed orthogonal to the flight envelope by  $L/(D+F_f+F_w^{gra})$ . Noting that in a closed loop trajectory the value of  $F_w^{gra}$  alternates, the equation is modified in calculating the mechanical power of the system, and further expressed in terms of  $G_e$  (2.10):

$$|\bar{V}_C| = V_{||} \frac{L}{D+F_f} = G_e V_{||} \quad (2.13)$$

The vector  $V_{||}$  can be expressed in terms of the angle from the horizontal  $\vartheta$ , the azimuth<sup>8</sup> angle  $\phi$ , and the reel out velocity  $\bar{V}_L$ . The refined crosswind motion law can therefore be written as [24]:

$$|\bar{V}_C| = G_e |\bar{V}_w \cos \vartheta \cos \phi - \bar{V}_L| \quad (2.14)$$

This analysis is continued, considering the effect of a rigid sloping tether, and neglecting minor corrective terms, the maximum mean mechanical power is found to be:

$$P = \frac{1}{2} \rho_a A V^3 C_L \frac{4}{27} G_e^2 \cos^3 \vartheta_0 \quad (2.15)$$

Where  $\vartheta_0$  is the mean angle of the tether with the horizontal. In this paper, the tether is modeled as inelastic, and its drag is calculated through a slightly modified equation (2.11), replacing apparent wind velocity  $V_a$  with crosswind velocity  $\bar{V}_C$ . The effective glide ratio is thus calculated by:

$$G_e = \frac{C_L}{C_D + \frac{C_{D,t} r d_t}{4A}} \quad (2.16)$$

Where  $C_{D,t}$  is the drag coefficient for flow normal to the tether and  $A$  is the kite reference area.

### 2.3 Tether Flexibility

Tether drag was initially modelled as a rigid tether with a uniform wind velocity profile in equation (2.11). However, this contrasts with the physical kite-tether system, where it's observed that the tether mainly follows the kite's motion at its highest point. A recent thesis on a Kitegen stem energy device considered the impact of tether flexibility on tether drag [24].

The position of the tether during the flight is found by solving a dynamic system accounting for the main forces on the cable. Applying Newton's second law to the tether, the following equation of motion is obtained:

$$\mu \ddot{a} = \frac{dT}{ds} + \bar{w} + \bar{f}_t \quad (2.17)$$

Where  $\mu$  is the tether's linear density,  $\ddot{a}$  is its acceleration,  $T$  is the variable tension along the tether,  $s$  is the abscissa identifying position along the tether,  $\bar{w}$  is the tether weight, and  $\bar{f}_t$  is the aerodynamic drag acting on the tether.

The problem is numerically solved by discretising both space  $s$  and time  $t$ , using the finite difference method to approximate derivatives. The assumption of constant kite velocity is applied as a boundary condition. Notably, the tether drag coefficient is considered variable, determined by the Reynolds number, a function of the position along the tether  $s$ , air density  $\rho_a$  and wind velocity  $V_w$ .

This analysis showed that the total aerodynamic drag of the tether for a rigid tether as expressed in equation (2.11) varied essentially linearly with tether length, while the aerodynamic drag of a flexible tether had an asymptotic relation to tether length, as shown in Figure 6.

---

<sup>8</sup>Referring to the horizontal angle in spherical coordinates

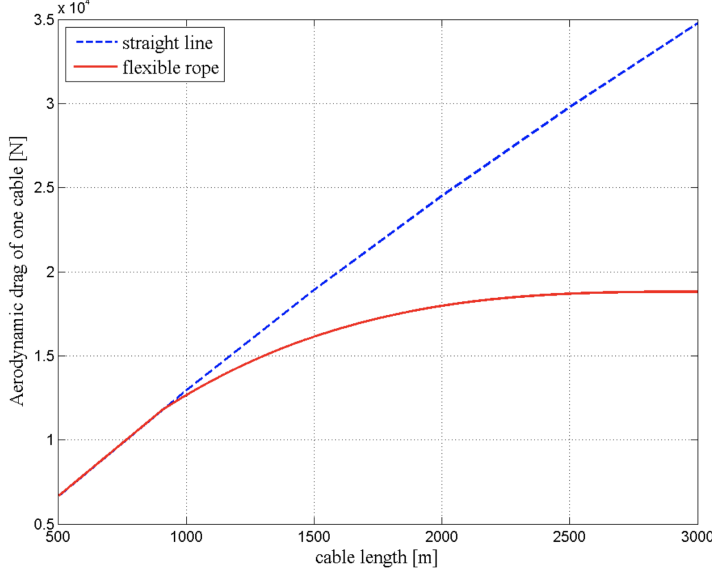


Figure 6: Aerodynamic drag acting for a rigid and flexible tether, at varying tether length [24].

To assess this impact on mechanical power output, both tether drags are added directly to kite drag, defining  $G_e$  as:

$$G_e = \frac{L}{D + 2F_t} \quad (2.18)$$

The power output for varying tether lengths was evaluated, modelling air density and wind velocity with equations (1.4) and (1.5). This analysis showed that with increased tether length, a flexible tether model produced significantly more power than a rigid tether. However, the rising wind velocity at longer tether lengths did not offset the effect of tether drag on  $G_e$ , resulting in a decrease in power output with increasing tether length regardless of the tether model, as depicted in Figure 7.

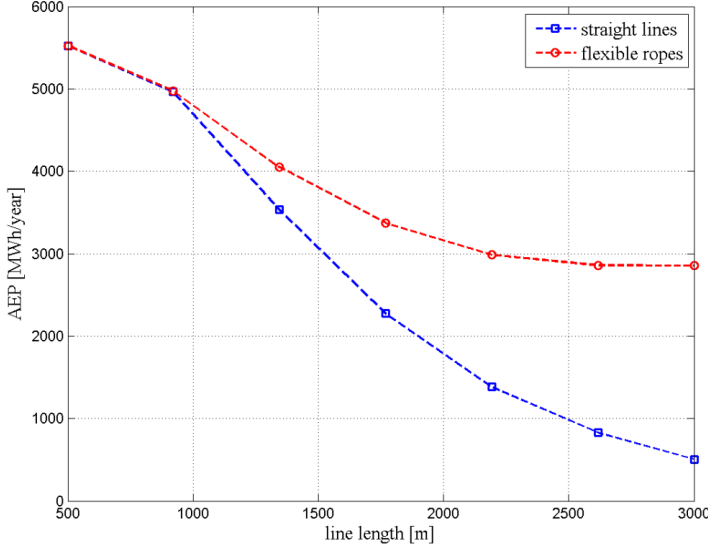


Figure 7: Annual energy production for a rigid and flexible tether, at varying tether length [24].

## 2.4 Review of Assumptions

The refined crosswind motion laws described in section 2.2, and its associated  $G_e$ , have been further developed and utilised in a number of academic works. In [23], corrective coefficients  $k_0$  and  $k_*$  are introduced to account for geometrical approximations, and gravitational, centrifugal, and friction forces. Numerically, these coefficients gave a correction of 0.3% and 0.8% respectively. In a continued analysis, [25] considers a variable  $G_e$  in a closed-loop flight, appending performance coefficient  $\eta^*$  to equation (2.15). In [26] and [27], inertia is taken into account, analysing the power output in traction power and a PKG respectively, both mentioning that the integral tether drag can be added to kite drag. Actuator disk theory is applied to crosswind kite systems in [28], appending the term  $(1-a)^2$  to equation 2.15, the induction factor  $a$  which can be found from the aerodynamic efficiency and solidity factor.

The majority of numerical analyses in crosswind kite power applications utilise the effective glide ratio,  $G_e$ , in power calculations. Tether dynamics' implications on tether drag and system motion have been largely overlooked in the literature, with most models assuming a straight-line tether and calculating  $G_e$  using (2.16). The effect of tether sag was studied analytically in [29] and numerically in [30], while the implication of tether dynamics on tether drag was explored numerically in section 2.3 [24]. The assumption that tether drag directly contributes to kite drag has rarely been questioned since the introduction of  $G_e$  in [22], and is asserted numerous times in the first and only textbook on airborne wind energy [4]. Due to the inclusion of tether drag in the effective glide ratio and its quadratic relationship with power shown in equation (2.15), tether drag has been identified as a core issue to AWE efficiency [15], with some dual airfoil designs proposed specifically to reduce tether drag [31] and European Commission reports citing tether drag multiple times as a core issue to the commercialisation of AWE [32].

In light of experimental observations, the widespread acceptance of  $G_e$  has been challenged by KiteGen, to little avail [19][33]. Unlike initial models of tethered airfoils as depicted in Figure 5, where the tether attachment has 3 rotational degrees of freedom, a KiteGen Stem kite is pinned to the tether by a bridle<sup>9</sup>, as shown in Figure 8. This essentially keeps the trim angle<sup>10</sup> constant, and allows for tether induced moments on the kite.

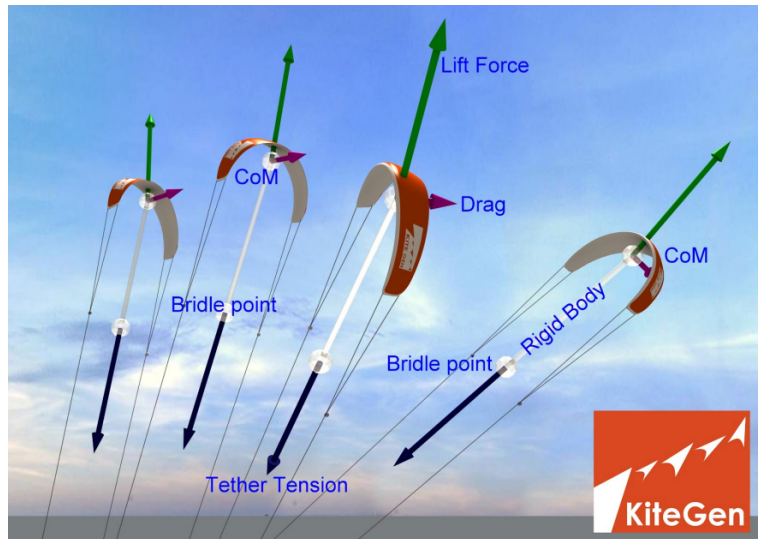


Figure 8: Illustration of KiteGen kite in motion, showing bridle attachment and major forces [20].

<sup>9</sup>System of lines attached to the kite.

<sup>10</sup>Angle formed between the kite and tether.

Reasonably assuming negligible effect of kite mass, the vector sum of aerodynamic forces and the tether tension as seen in Figure 8 must be balanced in magnitude and space. It thus becomes clear that the tether tension can never act against the kite's direction of motion, and therefore can never contribute to kite drag. It is also important to note that a flexible tether can only transfer tensile forces, and not shear forces, therefore the induced drag along the length of the tether cannot contribute to kite drag either. Understanding of these two observations lead to the rejection of the absurd notion that tether drag contributes directly to aerodynamic drag, a gross oversimplification of the system being analysed.

Evidently, the energy loss due to tether drag will have an effect on system efficiency. In reality, the aerodynamic drag acting on the tether will solely affect the magnitude and direction of the tether tension, which will induce a moment on the kite, due to the bridle point being offset from the center of mass. This will have a purely geometrical effect on the flight path, affecting the orientation of the kite with respect to the wind, as well as the maximum crosswind distance a kite can travel before looping.

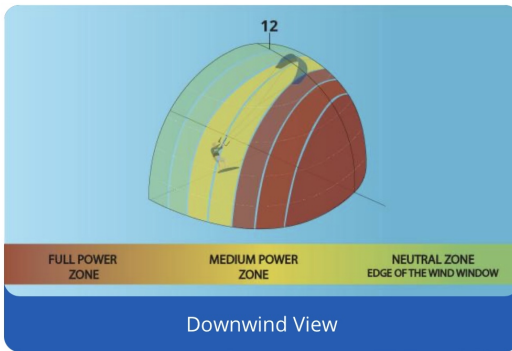
### 3 Project Plan

#### 3.1 Project Outline

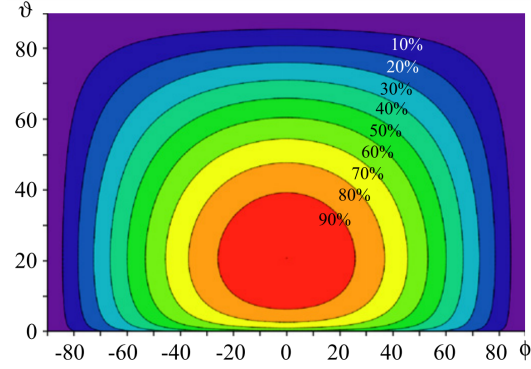
An updated analytical model of crosswind kite power is necessary to rectify the underlying false assumption that tether drag contributes to kite drag and to provide an analytical explanation of the true impact of tether drag on system dynamics. This project will have the following key objectives:

- Demonstrate the current tether drag assumption is flawed, and reject the effective glide ratio parameter  $G_e$ .
- Develop a new analytical model for power generation of a KiteGen Stem pumping kite generator, considering tether drag effects on system dynamics.
- Numerically apply the new analytical model and validate with experimental data.
- Explore the implications of the new analytical model on ideal tether length, system efficiency, and economics.

In order to explain the geometrical impact of tether weight and drag on power output and therefore system efficiency, two key concepts must be considered. The idea of cosine losses, shown in equation (2.15), was introduced in [23], stating that instantaneous power  $P \propto \cos^3(\vartheta)$ , where  $\vartheta$  is the angle between the wind and the flight envelope. This relation is closely linked to the concept of the wind window<sup>11</sup>, shown in Figure 9, demonstrating how instantaneous power varies within the flight envelope with the angle from the horizon  $\vartheta$  and azimuth angle  $\phi$ .



(a) Illustration of the power zones in the wind window during kitesurfing [34].



(b) Iso-power lines in the wind window considering varying wind velocity with altitude [25].

Figure 9: Visual representation and numerical calculation of power zones in the wind window.

In contrast to simple straight-line tether models (as seen in [25]), the flight envelope, and thus the wind window, does not remain centred around the ground station. With shorter tethers, it's reasonable to assume a straight-line path, but as tether length increases, flexibility comes into play and significantly influences the shape and position of the wind window. Instead of the flight envelope diameter expanding linearly with length, it tends to grow in a more asymptotic fashion, similar to tether drag in section 2.3. It causes the wind window's starting point to shift away from the ground station, progressing up along the tether. Tether flexibility introduces further complexities by continuously altering the origin point within the closed-loop flight path, thereby disrupting the previously assumed quarter-sphere flight envelope [23].

---

<sup>11</sup>Common concept in kite-surfing.

### **3.2 Project Timeline**

This 7-month project can be divided into three main phases: analytical, validation, and exploration.

Analytical Phase (1<sup>st</sup> October - 27<sup>th</sup> January): This phase focuses on gaining a deeper understanding of the KiteGen Stem system, and proposing an updated analytical model for AWE power generation. The impact of kite orientation on aerodynamic efficiency will be explored, supported by experimental data to ensure the model's accuracy.

Validation Phase (15<sup>th</sup> December - 9<sup>th</sup> February): During this phase, the analytical model will be applied to a KiteGen Stem device, with numerical evaluations of system behaviour and power production. These results will be validated using experimental data to enhance the model's accuracy.

Exploration Phase (4<sup>th</sup> February - 2<sup>nd</sup> March): This phase involves exploring the impact of varying tether lengths on power output, with a focus on system efficiency and economic implications.

The success of this project depends on the accuracy of the proposed model, which requires in-depth research on analytical modelling of flexible tether behaviour and kite system dynamics. Achieving the goals outlined in section 3.1 will require guidance from KiteGen regarding system parameters and behaviour, and access to experimental data.

An on-site visit to KiteGen headquarters is planned, likely between 1<sup>st</sup> - 15<sup>th</sup> January, to facilitate understanding and collaboration. For a visual representation of the project's timeline and dependencies, please refer to the attached Gantt chart.

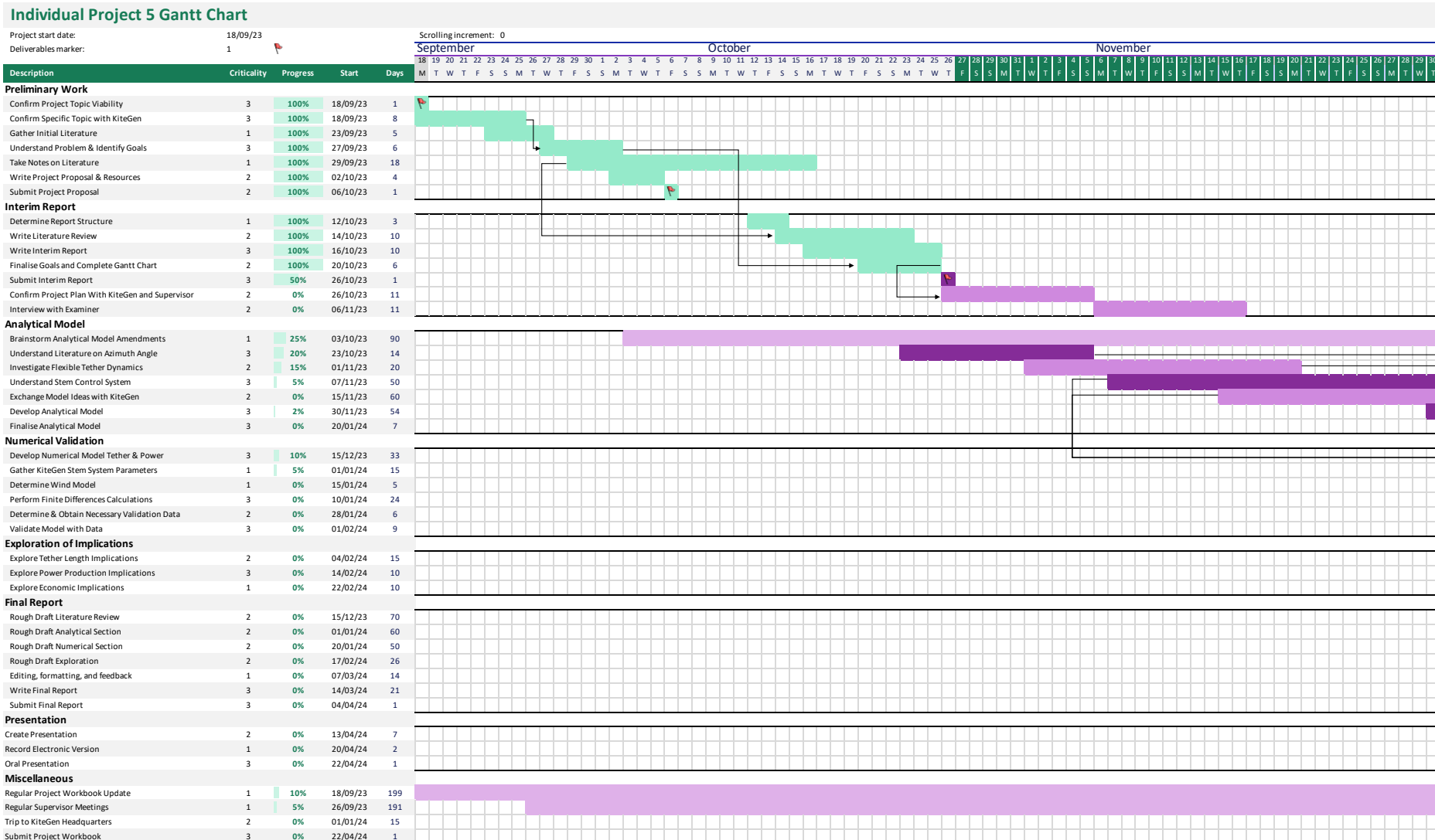


Figure 10: Gantt chart showing criticality and dependencies of activities, part 1 (18/09/2023 - 30/11/2023).

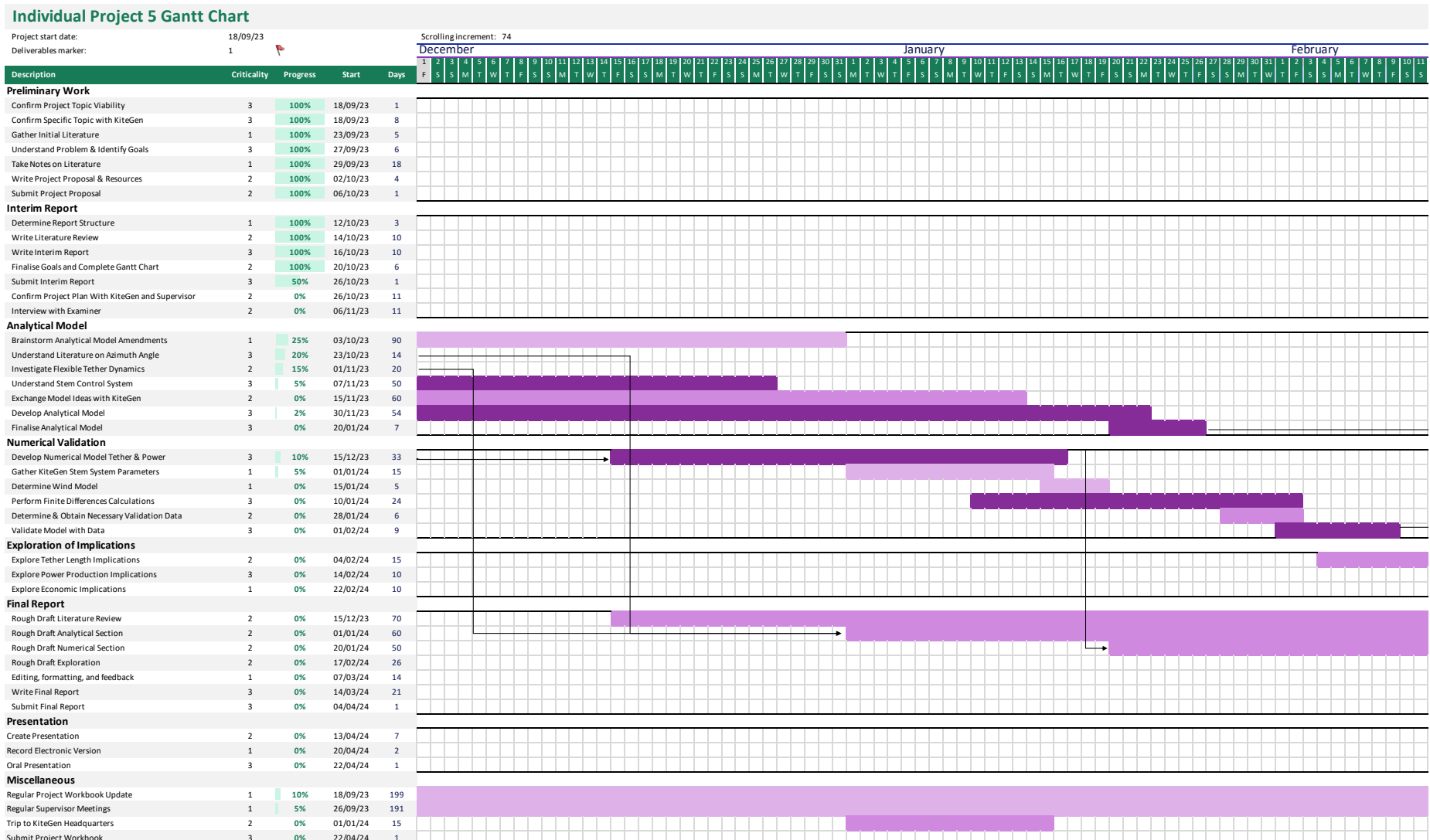


Figure 11: Gantt chart showing criticality and dependencies of activities, part 2 (1/12/2023 - 11/02/2024).

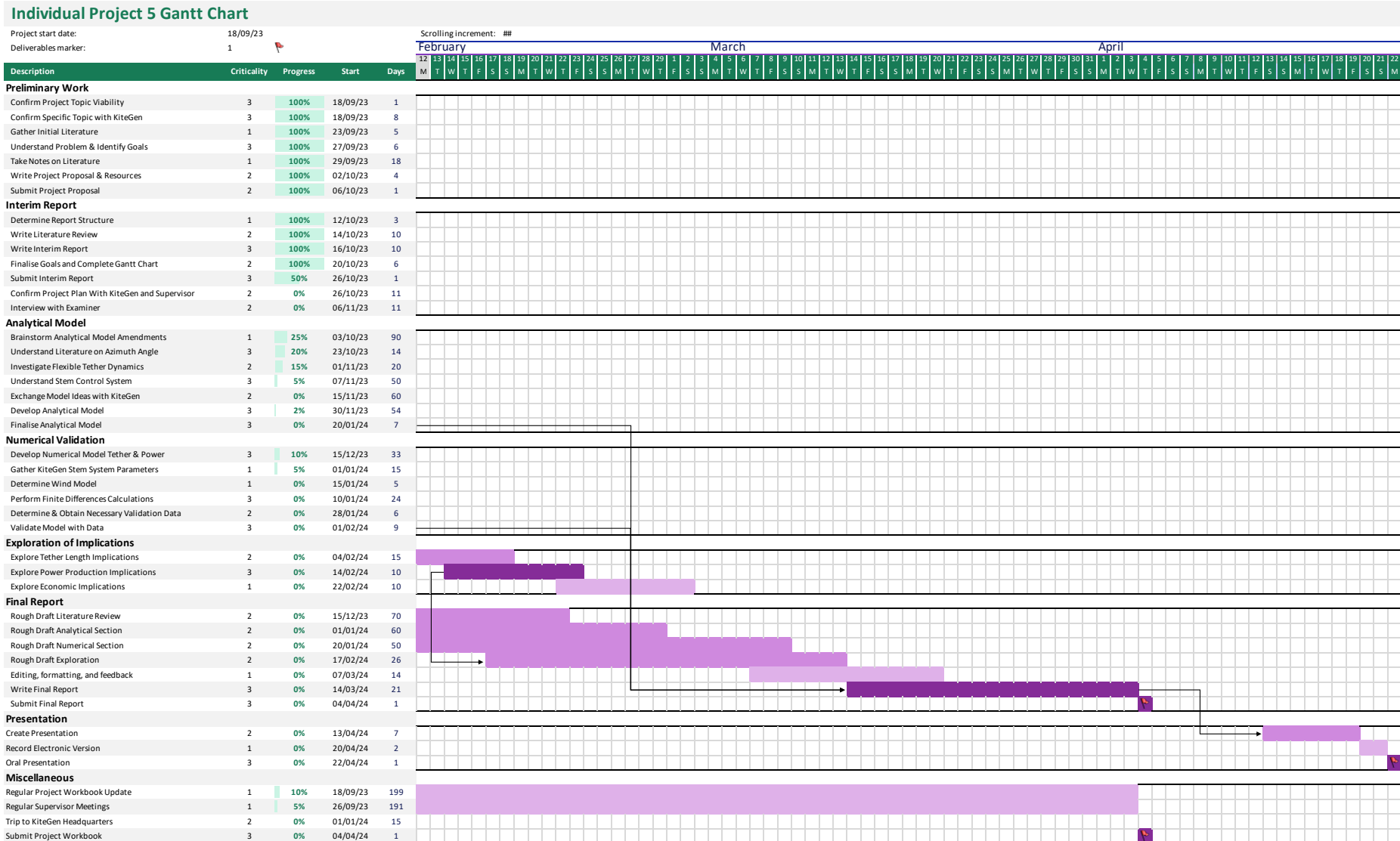


Figure 12: Gantt chart showing criticality and dependencies of activities, part 3 (12/02/2024 - 22/04/2023).

## References

- [1] Robert Carter. Boat remains and maritime trade in the persian gulf during the sixth and fifth millennia bc. *antiquity*, 80(307):52–63, 2006.
- [2] William Shepherd and Li Zhang. *Electricity generation using wind power*. World scientific, 2017.
- [3] Global Wind Energy Council. Global wind report 2023. *GWEC: Brussels, Belgium*, 2023.
- [4] Uwe Ahrens, Moritz Diehl, and Roland Schmehl. *Airborne wind energy*. Springer Science & Business Media, 2013.
- [5] Boris Houska and Moritz Diehl. Optimal control for power generating kites. In *2007 European Control Conference (ECC)*, pages 3560–3567. IEEE, 2007.
- [6] Cristina L Archer and Ken Caldeira. Global assessment of high-altitude wind power. *Energies*, 2(2):307–319, 2009.
- [7] MR Gustavson. Limits to wind power utilization. *Science*, 204(4388):13–17, 1979.
- [8] Matthias Schmitz and Reinhard Madlener. Economic viability of kite-based wind energy powerplants with caes or hydrogen storage. *Energy Procedia*, 75:704–715, 2015.
- [9] Lorenzo Fagiano, Mario Milanese, and Dario Piga. High-altitude wind power generation. *IEEE Transactions on Energy Conversion*, 25(1):168–180, 2009.
- [10] Massimo Ippolito and Eugenio Saraceno. Kitegen research. *Response to ‘Jet stream wind power as a renewable energy source: Little power, big impacts*.
- [11] Fabrizio Bompiani. *Bilancio energetico dell’impianto” Kite Gen Stem”*. PhD thesis, 2009.
- [12] JN Heilmann. The technical and economic potential of airborne wind energy. Master’s thesis, 2012.
- [13] S Mann. An introduction to airborne wind technology and cost reduction trends. *An Introduction to Airborne Wind Technology and Cost Reduction Trends*, 2019.
- [14] Lorenzo Fagiano. Control of tethered airfoils for high-altitude wind energy generation. *Polytechnico di Torino*, 2009.
- [15] Antonello Cherubini, Andrea Papini, Rocco Vertechy, and Marco Fontana. Airborne wind energy systems: A review of the technologies. *Renewable and Sustainable Energy Reviews*, 51:1461–1476, 2015.
- [16] Miles L Loyd. Crosswind kite power (for large-scale wind power production). *Journal of energy*, 4(3):106–111, 1980.
- [17] Rolf Van Der Vlugt, Johannes Peschel, and Roland Schmehl. Design and experimental characterization of a pumping kite power system. *Airborne wind energy*, pages 403–425, 2013.
- [18] Uwe Fechner and Roland Schmehl. Model-based efficiency analysis of wind power conversion by a pumping kite power system. *Airborne wind energy*, pages 249–269, 2013.
- [19] Massimo Ippolito. Reaction paper to the recent ecorys study, 2019. Available at: [https://www.researchgate.net/publication/331715736\\_Reaction\\_Paper\\_to\\_the\\_Recent\\_Ecorys\\_Study\\_KI0118188ENNenpdf\\_Challenges\\_for\\_the\\_commercialization\\_of\\_Airborne\\_Wind\\_Energy\\_Systems](https://www.researchgate.net/publication/331715736_Reaction_Paper_to_the_Recent_Ecorys_Study_KI0118188ENNenpdf_Challenges_for_the_commercialization_of_Airborne_Wind_Energy_Systems).

- [20] Kitegen, 2023. Available at: <http://kitegen.com>.
- [21] Kitegen side-slip animation, 2009. Available at: [https://www.youtube.com/watch?v=Zl\\_tqnsN\\_Tc](https://www.youtube.com/watch?v=Zl_tqnsN_Tc).
- [22] Boris Houska and Moritz Diehl. Optimal control of towing kites. In *Proceedings of the 45th IEEE Conference on Decision and Control*, pages 2693–2697. IEEE, 2006.
- [23] I Argatov, P Rautakorpi, and R Silvennoinen. Estimation of the mechanical energy output of the kite wind generator. *Renewable Energy*, 34(6):1525–1532, 2009.
- [24] Felice Roselli. Study on the dynamics of the flexible cables of a kite-gen type of energy generator, Mar 2016.
- [25] Ivan Argatov and Risto Silvennoinen. Energy conversion efficiency of the pumping kite wind generator. *Renewable Energy*, 35(5):1052–1060, 2010.
- [26] Roland Schmehl, Michael Noom, and Rolf van der Vlugt. Traction power generation with tethered wings. *Airborne Wind Energy*, pages 23–45, 2013.
- [27] Rolf H Luchsinger. Pumping cycle kite power. In *Airborne wind energy*, pages 47–64. Springer, 2013.
- [28] Mojtaba Kheiri, Frédéric Bourgault, and Vahid Saberi Nasrabad. Power limit for crosswind kite systems. 2018.
- [29] Ivan Argatov, Pauli Rautakorpi, and Risto Silvennoinen. Apparent wind load effects on the tether of a kite power generator. *Journal of Wind Engineering and Industrial Aerodynamics*, 99(10):1079–1088, 2011.
- [30] Rolf van der Vlugt, Anna Bley, Michael Noom, and Roland Schmehl. Quasi-steady model of a pumping kite power system. *Renewable Energy*, 131:83–99, 2019.
- [31] Mario Zanon, Sébastien Gros, Joel Andersson, and Moritz Diehl. Airborne wind energy based on dual airfoils. *IEEE Transactions on Control Systems Technology*, 21(4):1215–1222, 2013.
- [32] K Hussen, E Dietrich, J Smeltink, et al. Study on challenges in the commercialisation of airborne wind energy systems. Technical report, ECORYS Report PP-05081-2016, Brussels: European Commission, 2018.
- [33] Giancarlo Abbate and Eugenio Saraceno. The largest renewable, easily exploitable, and economically sustainable energy resource. *Europhysics News*, 49(1):16–22, 2018.
- [34] Iko, 2023. Available at: <https://www.ikointl.com/>.